Available online at www.ijournalse.org

Emerging Science Journal

(ISSN: 2610-9182)

Vol. 5, No. 3, June, 2021

Vertical Characteristics of Raindrops Size Distribution over Sumatra Region from Global Precipitation Measurement Observation

Ravidho Ramadhan [1], Marzuki [1*], Harmadi [1]

[1] Department of Physics, Universitas Andalas, Padang 25163, Indonesia

Abstract

The climatology of the vertical profile of raindrops size distribution (DSD) over Sumatra Region (10° S – 10° N, 90° E – 110° E) has been investigated using Global Precipitation Measurement (GPM) level 2 data from January 2015 to June 2018. DSD's vertical profile was observed through a vertical profile of corrected radar reflectivity (Z_e) and two parameters of normalized gamma DSD, i.e., mass-weight mean diameter (D_m) and total drops concentration (N_w). Land-ocean contrast and rain type dependence of DSD over Sumatra were clearly observed. The values of D_m and N_w were larger in the land than in the ocean. Negative and positive gradients of D_m toward the surface were dominant during stratiform and convective rains, respectively, consistent with the Z gradient. Moreover, the negative gradient of stratiform rain in the ocean is larger than in land. Thus, the depletion of large drops is dominant over the ocean, which is due to the break-up process that can be observed from the increase of N_w. Raindrop growth of convective rains is more robust over the ocean than land that can be seen from a larger value of D_m gradient. The BB strength is slightly larger over land and coastal region than over the ocean, indicating that the riming process is more dominant over land and coastal regions than the ocean.

Keywords:

Raindrop Size Distribution (DSD);
GPM; Sumatra;
Stratiform;
Convective.

Article History:

Received:	06	February	2021
Revised:	28	April	2021
Accepted:	08	May	2021
Published:	01	June	2021

1- Introduction

Raindrops size distribution (DSD) is essential to understand the physical process of rainfall events [1]. It can reflect the processes experienced by the raindrop as they fall to the ground. By knowing the vertical profile of DSD, we can understand the microphysical process of drop evolution [2-4]. Moreover, knowledge of DSD is also used to estimate rain attenuation in telecommunication technology using microwave [5-7] and design space-based precipitation radar system [8, 9].

The vertical profile of DSD varies in space and time that can influence the application of DSD. For example, constant DSD is commonly used to derive the *Z-R* relationship for weather radar data conversion. This would be less accurate to estimate rainfall because of the variation of the vertical structure of DSD [10-12]. There are some DSD variability such as regional variability [13, 14], rainfall type [15, 16], diurnal variability [6, 17, 18], seasonal variability [19-20], and intraseasonal variability [21].

Surface-based radar is the most common instrument to observe DSD's vertical profile, but it has some limitations, particularly regarding observation coverage. To overcome the limitation of surface radar, satellite-based radar or spaceborne radar can be another option that can cover broader observational areas. Before 2014, we do not have any satellite-based radar capable of observing DSD until Global Precipitation Measurement (GPM) was launched in

* **CONTACT**: Marzuki@sci.unand.ac.id

DOI: http://dx.doi.org/10.28991/esj-2021-01274

February 2014 [22]. The GPM is an advanced Tropical Rainfall Measuring Mission (TRMM) project that provides some precipitation parameters, including DSD parameters.

This work uses GPM data to investigate the vertical characteristics of DSD over Sumatra region. Sumatra is located in the tropical region's warm pool, which is the most active convective area in the world [23]. Several studies have been conducted to study the vertical profile of DSD over Sumatra [18, 24, 25]. Renggono et al. [24] observed DSD's vertical profile using Equatorial Atmospheric Radar (EAR). Marzuki et al. [25] and Ramadhan et al. [18, 20] observed the vertical profile of DSD using Micro Rain Radar (MRR). Using this instrument, they found the rainfall type and diurnal variation of DSD in Sumatra. However, all previous studies were only conducted at one location, namely, at the Equatorial Atmosphere Observation, which is located in Kototabang, West Sumatra (0.20°S, 100.32°E; 865 m above sea level). Therefore, to describe DSD's vertical characteristics over the whole Sumatra Region, we used the data of GPM level 2. The GPM data provide two parameters of normalized gamma DSD, i.e., mass-weight mean diameter (D_m) and total drops concentration (N_w). The performance of GPM to estimate the DSD parameters has been examined by several studies [26-28].

2- Data and Methodology

The region of interest is Sumatra and the surrounding ocean (10° S – 10° N, 90° E – 110° E). The GPM level 2 data of the study area from January 2015 to June 2018 are used. GPM carries Dual-Frequency Precipitation Radar (DPR) that was Ku-band (13.6 GHz) and Ka-band (35.5 GHz) frequency radar [22, 29]. The type of DPR scanning proceeds three modes of data, i.e., Normal Scan (NS), Match Scan (MS), and High-sensitivity Scan (HS). This mode is produced from different scanning in which NS is from Ku-band scanning while MS and HS are from Ku and Ka combinations. Although NS was produced only from Ku-band scanning, previous studies show good performance of NS scanning for DSD observation in comparison with a ground radar [28, 30]. Ku band has 125 m vertical resolution with 176 range bin and 49 swath with 5×5 km resolution approximately.

The GPM DPR level 2 data are classified into convective and stratiform rains using the classification method, which is available in the classification (CSF) module of GPM [31]. The GPM algorithms consist of the preparation (PRE) module, the vertical (VER) profile module, the classification (CSF) module, the drops size distribution (DSD) module, the surface reference technique (SRT) module, and the solver (SLV) module [32]. This paper used GPM level 2 data version 5 (V05) that was released in May 2017. This version included precipitation at the surface and additional parameters like some parameters and flag, freezing level altitude, and land surface type [33]. The CSF modules used in this study were type precipitation, quality BB, quality rain type precipitation, height BB, bin of BB top, and bin of BB bottom. We only analyze the data if quality BB and quality rain type precipitation are 1. Finally, we also used the precipitation near surface, Z factor corrected (Z_e), and DSD parameter data, which are obtained from the SLV module.

GPM provides mass-weight mean diameter (D_m) in mm and total drops concentration (N_w) in dBN_w unit. These parameters are belong to normalized gamma distribution [34] expressed by:

$$N(D) = N_w f(\mu)\left(\frac{D}{D_m}\right)^{\mu} exp\left[-(4+\mu)\frac{D}{D_m}\right], \tag{1}$$

where D is drops diameter in mm, $N(D)$ is the number of density in $m^{-3}mm^{-1}$, and $f(\mu)$ is a function of shape parameter (μ):

$$f(\mu) = \frac{6}{256}\frac{(4+\mu)^{\mu}}{\Gamma(\mu+4)}. \tag{2}$$

Parameter N_w in mm^{-3} is the ratio between liquid water content (W) in gm^{-3} and parameter D_m [35], while D_m is the ratio for the fourth to third moment from DSD. The parameter N_w is expressed by:

$$N_w = \frac{256}{\pi\rho_w}\frac{10^3 W}{D_m^4}, \tag{3}$$

where ρ_w is the density of water in gm^{-3}. This study does not retrieve the DSD parameters manually, we use D_m and N_w that the GPM has been provided. These parameters were calculated from the rainfall rate (R)-D_m relationship that tends to Z_e observation [36]. Details theoretical basis of this algorithm can be seen in Iguchi et al. [37].

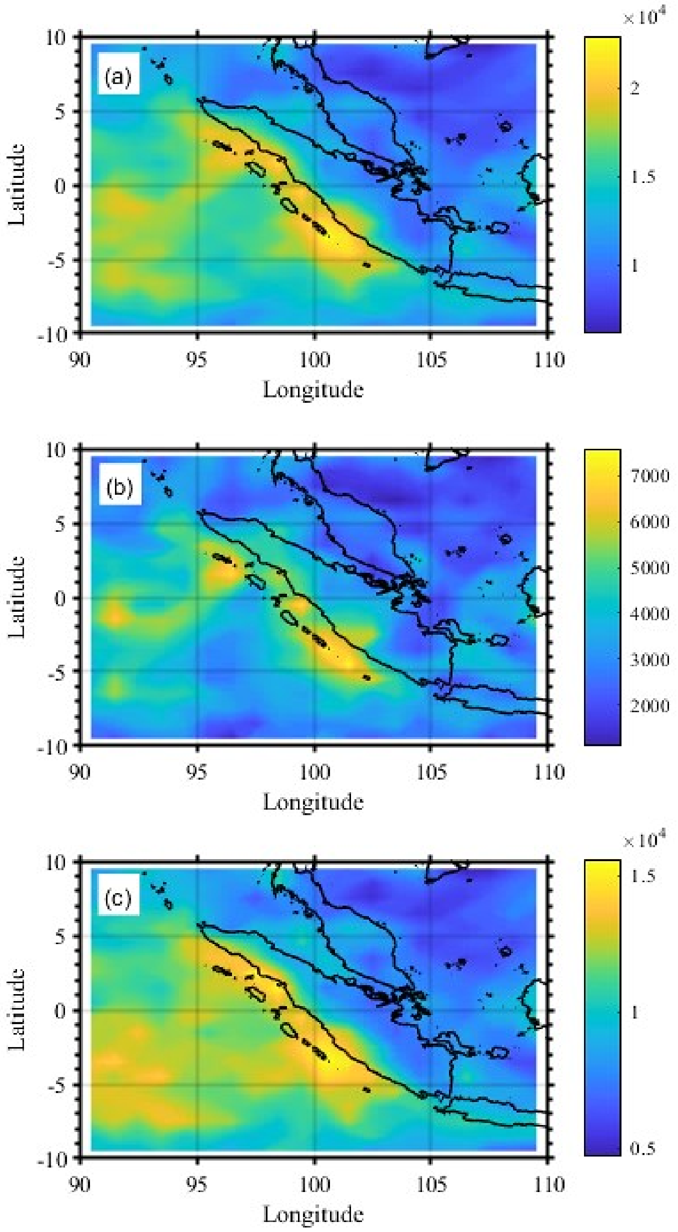

Figure 1. Spatial distribution of GPM level 2 data for a) all rainfall types, b) stratiform rain, and c) convective rain.

This study investigated the vertical structure of DSD over the Sumatra region by filtering the data for near-surface rainfall greater than 0.1 mm/h. We used the precipitation classification from the GPM level 2 data to divide rainfall types into stratiform and convective rain. The spatial distribution of data was given in Figure 1. It contained 5,325,630 data for all rainfall event (Figure 1a), 1,389,261 data for stratiform rain (Figure 1b), and 3,936,369 data for convective rain (Figure 1c). Usually, the number of stratiform rain profiles is the largest [18, 20], but we found the stratiform rain profile is smaller than convective rain in this study. We compared both stratiform and convective DSD characteristics for several locations, including land, coastal, strait, and ocean, to find the variability.

3- Results

Figure 2 shows the spatial distribution of the vertical profile of reflectivity gradient (VPRG) above and below the melting layer. It can be used to identify the growth of hydrometeors. Above the melting layer, the gradient was calculated in 5-7 km rain column, while below the melting layer, the VPRG was calculated at the altitude of 1-3 km. All gradients above the melting layer are positive (downward increasing toward the surface, hereafter DI) both for both stratiform and convective rain (Figures 2a and 2c).

Stratiform rain has larger DI above melting layer than convective rain, consistent with characteristics of the convective-stratiform formation. Although DI above the melting layer is positive for convective and stratiform, below the melting layer, stratiform has negative VPRG, while convective rain has positive values.

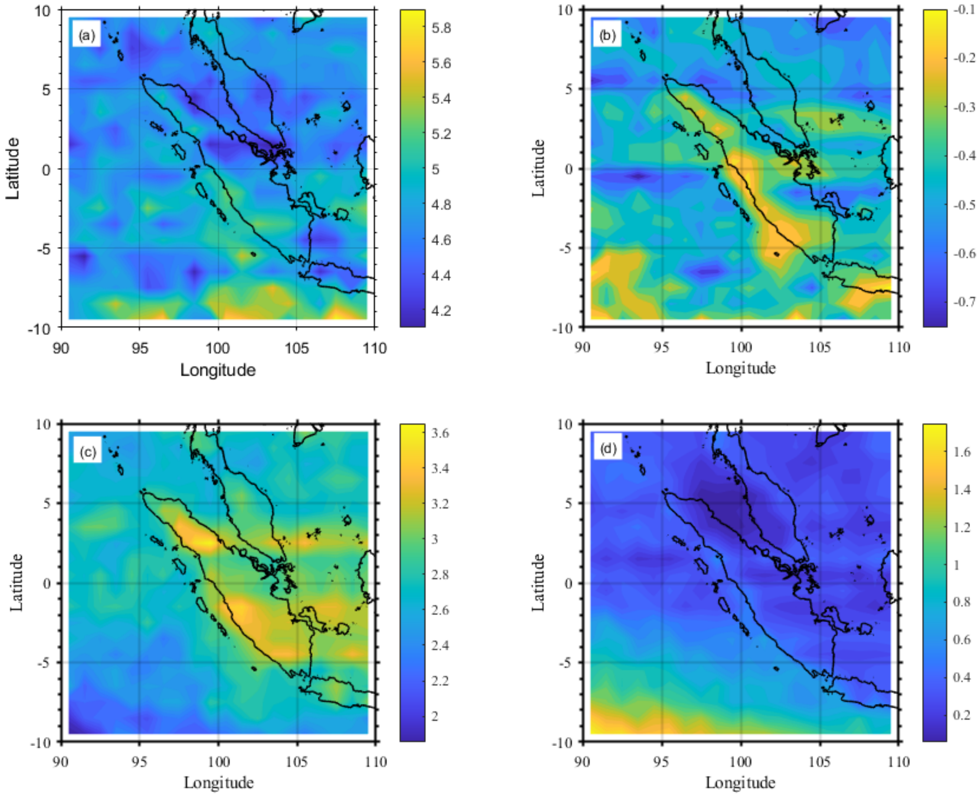

Figure 2. Spatial distribution of vertical profile of reflectivity gradient (VPRG) for stratiform rain at the altitude of 5 - 7 km (a), and 1 - 3 km (b), and convective rain at the altitude of 5 - 7 km (c), and 1 - 3 km (d).

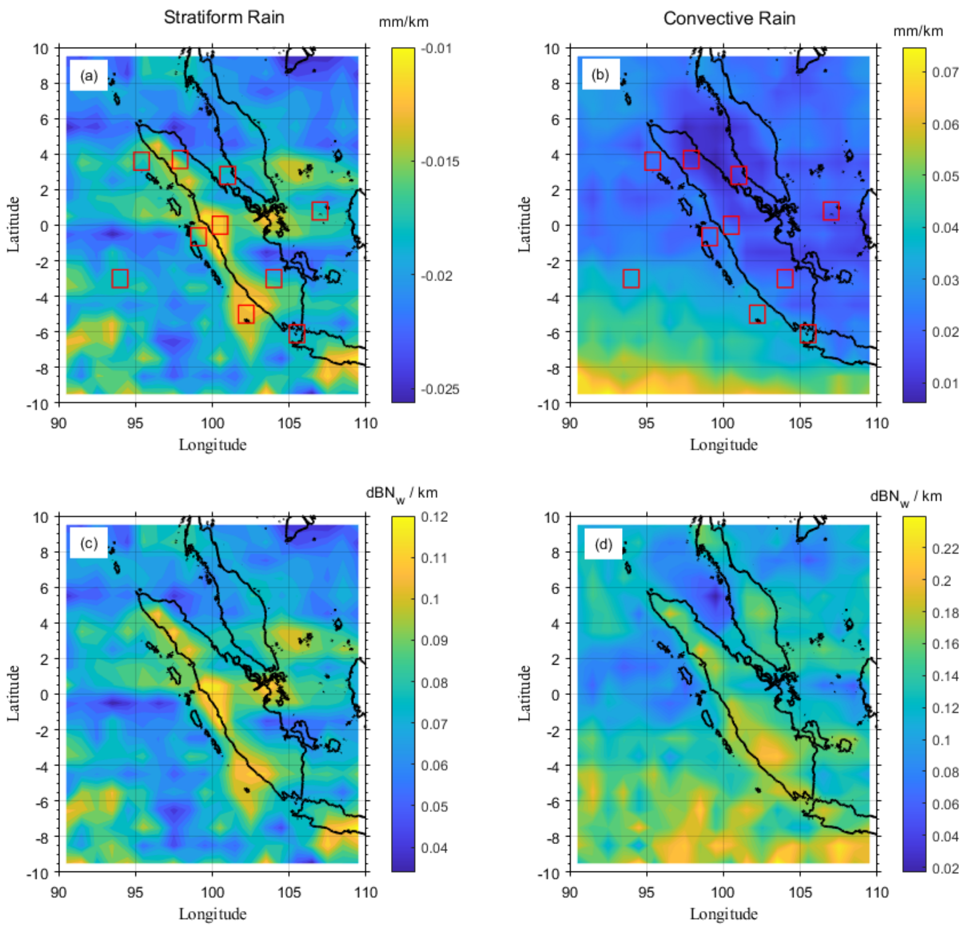

Figure 3. Spatial distribution of vertical gradient of D_m for stratiform (a) and convective (b) rains, and for N_w (c and d). The gradient was calculated at the altitude of 1.5 - 4 km.

VPRG for stratiform and convective rains show a regional variation. Above the melting layer, the stratiform's DI gradient is larger over the ocean than over land (Figure 2a). A slightly larger DI gradient of stratiform rain over the land was observed on Sumatra's western coast, which is consistent with the previous study in Indonesia Maritime Continent (IMC) [38, 39]. Otherwise, the DI gradient of convective rain is larger over the land than over the ocean, especially in the western region of Sumatra (Figure 2c). Thus, the growth of hydrometeor for convective rain is more robust over land, while for stratiform rain, it is more dominant over the ocean [40]. A larger positive DI gradient (positive VPRG) is observed below the melting layer during convective rain over the ocean, indicating that the increase of large-size drops concentration is more significant over the ocean. On the other hand, stratiform rain shows a larger negative gradient of VPRG over this region (Figure 2b), indicating the decrease of large-size drops concentration, consistent with the D_m gradient for the below-melting layer (Figure 3).

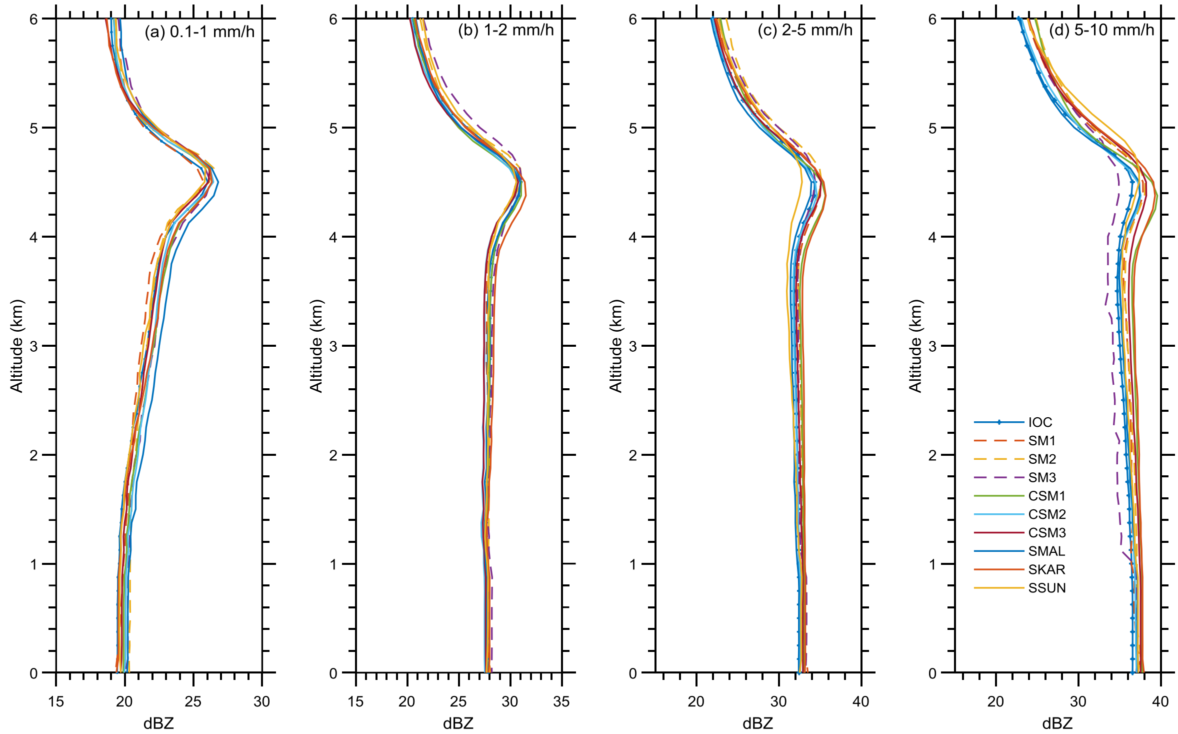

Figure 4. Vertical profile of reflectivity factor (*Z*) for ten selected locations of stratiform rain for a) very light rain, b) light rain, c) moderate rain, and d) heavy rain.

Gradients of D_m and N_w for stratiform and convective are given in Figure 3. The gradients were calculated in the rain column 1.5-4.0 km. A negative gradient was observed for the vertical profile of D_m during stratiform rain (Figure 3a). It means there is a decrease of large-sized drops toward the surface during stratiform rain over Sumatra region, which is consistent with the VPRG trend (Figure 2b). The decreasing D_m trend for stratiform rain is followed by N_w's increase that indicates the break-up process [42]. This result is different from previous studies at Kototabang in west Sumatra using MRR [18, 20, 42]. It may be due to a small-scale variability of vertical DSD over Sumatra. Therefore, we analyze the DSD for ten selected locations include Kototabang in Section 3.1.

Table 1. Distribution of data for several locations of stratiform rain from GPM observation.

No.	Name	Location	Total Data					
			$0.1 \leq R<1$	$1 \leq R<2$	$2 \leq R<5$	$5 \leq R<10$	$10 \leq R<20$	$\dot{R} \geq 20$
1	Indian Ocean (IOC)	2.5° - 3.5°S, 93.5° - 94.5°E	2170	946	1046	292	2170	946
2	Sumatra 1 (SM1)	3.19° - 4.19° N, 97.4° - 98.4°E	2368	1123	1156	252	2368	1123
3	Sumatra 2 (SM2)	0.5° S - 0. 5° N, 100° - 101° E	1872	777	685	162	1872	777
4	Sumatra 3 (SM3)	3.5° - 2.5° S, 103.5° - 104.5° E	937	398	300	26	937	398
5	Coastal Sumatra 1 (CSM 1)	3.1° - 4.1° N, 94.9° - 95.9° E	2556	1182	1432	654	2556	1182
6	Coastal Sumatra 2 (CSM 2)	1.15° - 0.15° S, 98.6° - 99.6° E	2813	1338	1513	450	2813	1338
7	Coastal Sumatra 3 (CSM 3)	5.5° - 4.5° S, 101.7° - 102. 7° E	2735	1399	1858	827	2735	1399
8	Strait of Malacca (SMAL)	2.3° - 3.3° N, 100.5° - 101.5° E	1470	754	640	217	1470	754
9	Strait of Karimata (SKAR)	0.3° - 1.3° N, 106.5° - 107.5° E	1822	788	845	201	1822	788
10	Strait of Sunda (SSUN)	6.6° - 5.6° S, 105° - 106° E	829	323	342	137	829	323

Figure 3b and d show the spatial distribution of D_m and N_w gradients for convective rain. It can be seen that convective rain has a positive gradient for both D_m and N_w parameters, consistent with the VPRG pattern (Figure 2d). The D_m gradient is smaller over the land than over the ocean. This confirms a smaller increase of large drop concentration over land, as indicated by a small VPRG gradient (Figure 2d). The increase of D_m for convective rain coincides with an increase of gradient N_w. The increase of large-sized drops with the increasing total number of raindrops is likely due to several microphysical processes such as the accretion break-up and coalescence [41]. Break-up and coalescence processes occur during the convective rain over the ocean and land. However, the break-up processes are more dominant, especially over the ocean, indicated by a more significant increase of N_w.

3-1- Vertical Characteristics of Stratiform Rain

Figure 4 shows the vertical profile of the corrected radar reflectivity factor (Z_e) during stratiform rains from GPM observation for several locations over Sumatra. The selected area locations are given in Figures 3a and 3b, and the data distribution for these regions was presented in Table 1. The bright band (BB) appears for all rainfall intensities (R). To identify rainfall intensity dependence of vertical structure of stratiform precipitation, the data are classified into several classes of intensity i.e., very light rain ($0.1 \leq R < 1$), light rain ($1 \leq R < 2$), moderate rain ($2 \leq R < 5$), and heavy rain ($5 \leq R < 10$) [2]. We calculated the BB strength (ΔZ) by taking the difference in the average value of Z_e between Bright Band Height (BBH) and BB-bottom. The strength of BB is necessary to identify the number and size of the raindrop during their formation [43].

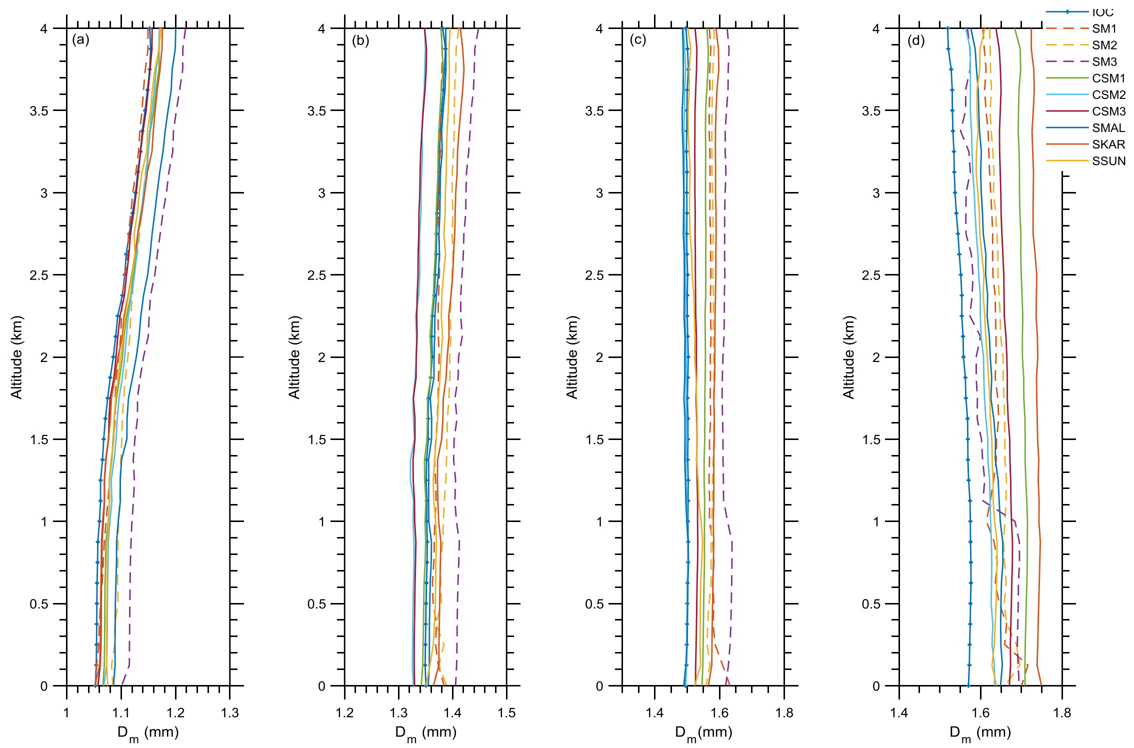

Figure 5. Vertical profile of mass-weight mean diameter (D_m) for ten selected locations of stratiform rain for a) very light rain, b) light rain, c) moderate rain, and d) heavy rain.

The BB strength (ΔZ) for each location is slightly different. The values of ΔZ (in dBZ) for very light rain are IOC (4.28), SM1 (4.50), SM2 (4.48), SM3 (4.15), CSM1 (4.04), CSM2 (4.27), CSM3 (4.14), SMAL (4.21), SKAR (4.09), and SSUN (4.12). Furthermore, ΔZ for heavy rain are IOC (2.62), SM1 (2.79), SM2 (2.89), SM3 (2.24), CSM1 (3.24), CSM2 (2.80), CSM3 (2.95), SMAL (3.06), SKAR (2.63), SSUN (2.41). Thus, very light rain has a larger ΔZ than heavy rain, which indicates a more dominant break up or riming process [44]. The strength of ΔZ is closely related to the decrease of large-sized drop soon after the ice crystal melts. There is a significant rain intensity dependence of VPRG below the melting layer. Very light rain has a negative gradient, while heavy rain has a positive gradient (Figure 4). This feature indicates the decrease of large-sized drops concentration during very light rain over Sumatra. The values of ΔZ during heavy rain for several coastal areas such as CSM1, CSM2, and CSM3 are larger than in other regions.

Figure 5 shows the vertical profile of D_m for all classes of stratiform rain. The values of D_m increase with an increasing rainfall rate. This is typical of DSD characteristics in the tropics [2, 14]. The value of D_m over land (SM1, SM2, SM3) is larger than other regions, indicating a smaller growth of raindrops over land than ocean, coastal, and strait, as observed in Figure 2. For very light to moderate rain, the larger value D_m was observed over land (SM2 and SM3). The larger D_m over land is associated with a smaller value of N_w (Figure 6). A similar pattern is also observed in the coastal region (CSM3). Thus, the DSD of stratiform rain over land comprises more large-sized drop concentrations with a small number of raindrop total. This fact is consistent with weak BB over land (Figure 4).

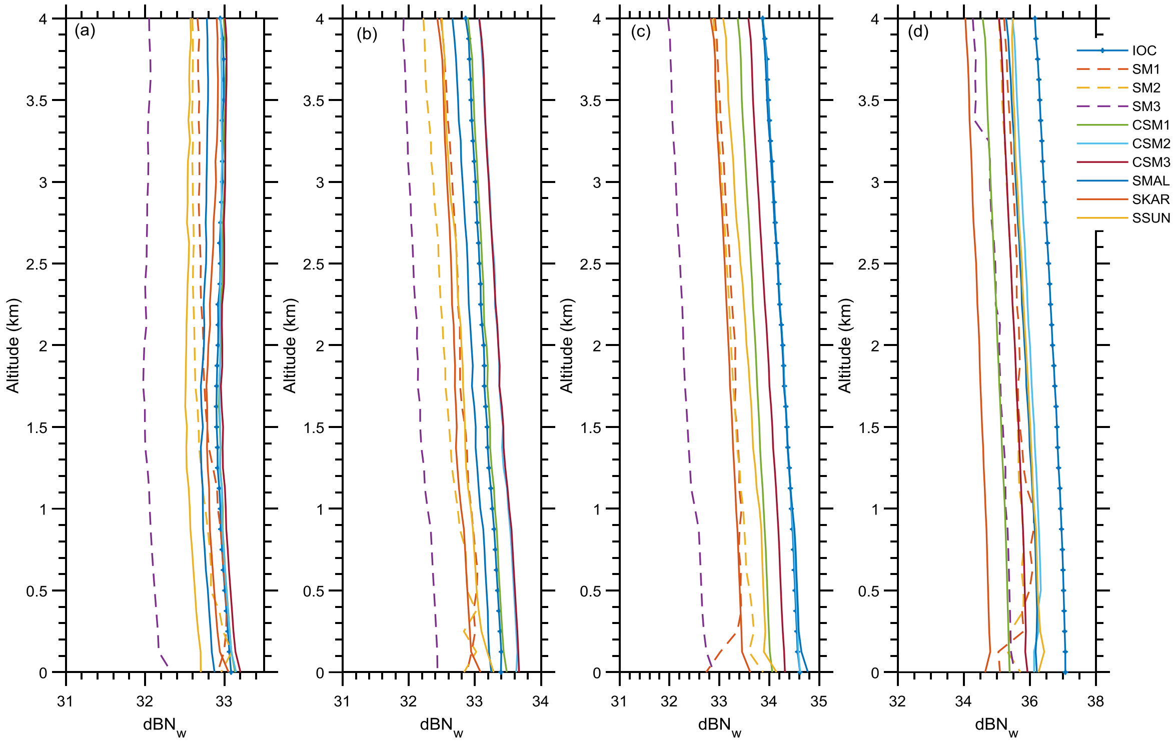

Figure 6. Vertical profile of total drop concentration (dBN_w) for ten selected locations of stratiform rain for a) very light rain, b) light rain, c) moderate rain, and d) heavy rain.

3-2- Vertical Characteristics of Convective Rain

Figure 7 shows Z_e's vertical profile during convective rains for several locations, which are indicated in Figures 3a and 3b. The data distribution for these regions was presented in Table 2. We classified convective rain into six rain intensities i.e. very light rain ($0.1 \leq R<1$), light rain ($1 \leq R<2$), moderate rain ($2 \leq R< 5$), heavy rain ($5 \leq R<10$), very heavy rain ($10 \leq R<20$), and extreme rain ($R \geq 20$) [2].

Table 2. Distribution of data for several locations of convective rain from GPM observation.

No.	Name	Location	Total Data					
			$0.1 \leq R<1$	$1 \leq R<2$	$2 \leq R<5$	$5 \leq R<10$	$10 \leq R<20$	$\grave{R} \geq 2\,0$
1	Indian Ocean (IOC)	2.5° - 3.5°S, 93.5° - 94.5°E	7298	2083	1940	655	390	481
2	Sumatra 1 (SM1)	3.19° - 4.19° N, 97.4° - 98.4°E	6486	2079	1931	709	284	246
3	Sumatra 2 (SM2)	0.5° S - 0. 5° N, 100° - 101° E	5112	1796	1588	544	263	144
4	Sumatra 3 (SM3)	3.5° - 2.5° S, 103.5° - 104.5° E	4089	1320	1082	346	140	107
5	Coastal Sumatra 1 (CSM 1)	3.1° - 4.1° N, 94.9° - 95.9° E	8070	2103	2042	-	402	437
6	Coastal Sumatra 2 (CSM 2)	1.15° - 0.15° S, 98.6° - 99.6° E	8137	2280	2228	842	412	456
7	Coastal Sumatra 3 (CSM 3)	5.5° - 4.5° S, 101.7° - 102. 7° E	7360	2186	2326	1068	572	570
8	Strait of Malacca (SMAL)	2.3° - 3.3° N, 100.5° - 101.5° E	5928	1693	1659	680	374	426
9	Strait of Karimata (SKAR)	0.3° - 1.3° N, 106.5° - 107.5° E	4815	1087	1050	432	193	179
10	Strait of Sunda (SSUN)	6.6° - 5.6° S, 105° - 106° E	4992	1516	1387	586	285	256

High rainfall intensity is associated with a larger positive VPRG above the melting layer. Below the melting layer, a positive gradient of Z_e was observed for almost all classes. The negative gradient of Z_e was observed only for very light rain (Figure 7a). Very light rain also shows a clear BB pattern in the melting layer (~5 km), which may indicate a miss classification of convective rain by the CSF module. The GPM is less sensitive to weak precipitation [45]. The gradient becomes positive when the rainfall intensity increases. The largest Z_e value was observed over land, and the smallest one was observed offshore (IOC). Although the largest Z_e value was observed over land, the VPRG value below the melting layer in this region is smaller (Figure 2). Thus, a larger raindrop size is found over land, but the raindrop growth is small in this region.

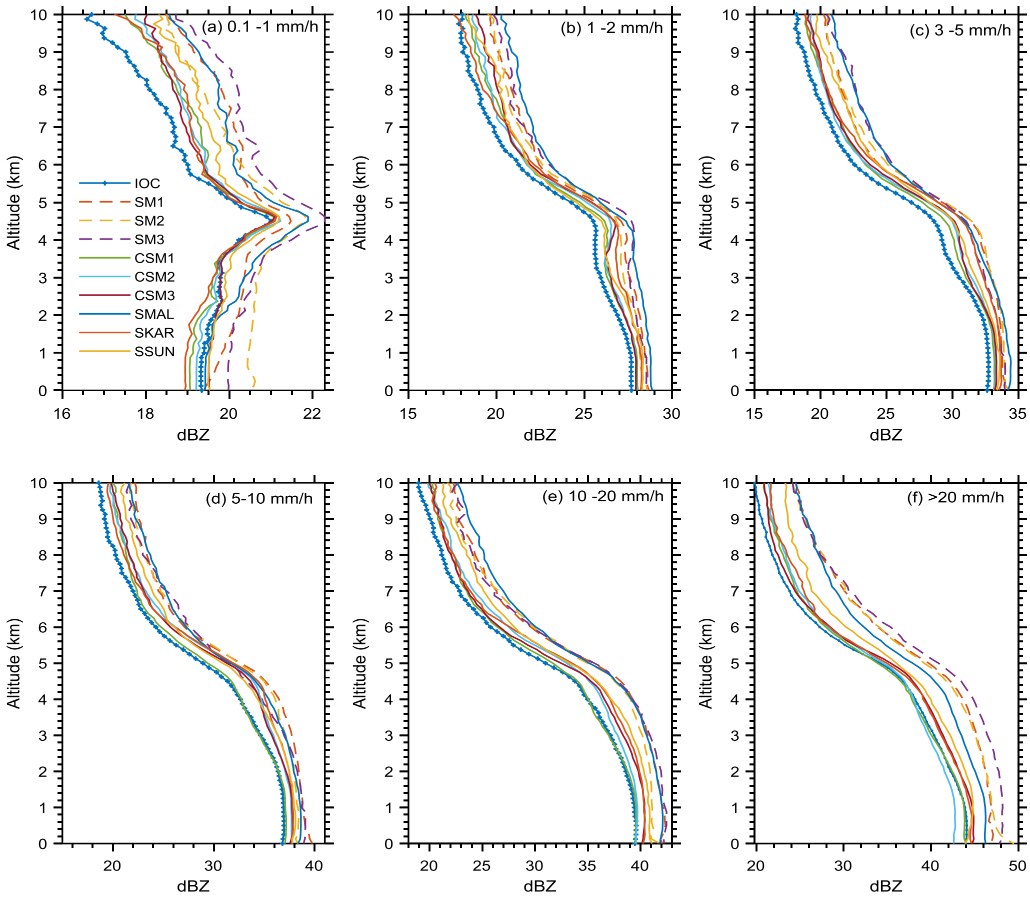

Figure 7. Vertical profile of reflectivity factor (*Z*) for ten selected locations of convective rain for a) very light rain, b) light rain, c) moderate rain, d) heavy rain, e) very heavy rain, and f) extreme rain.

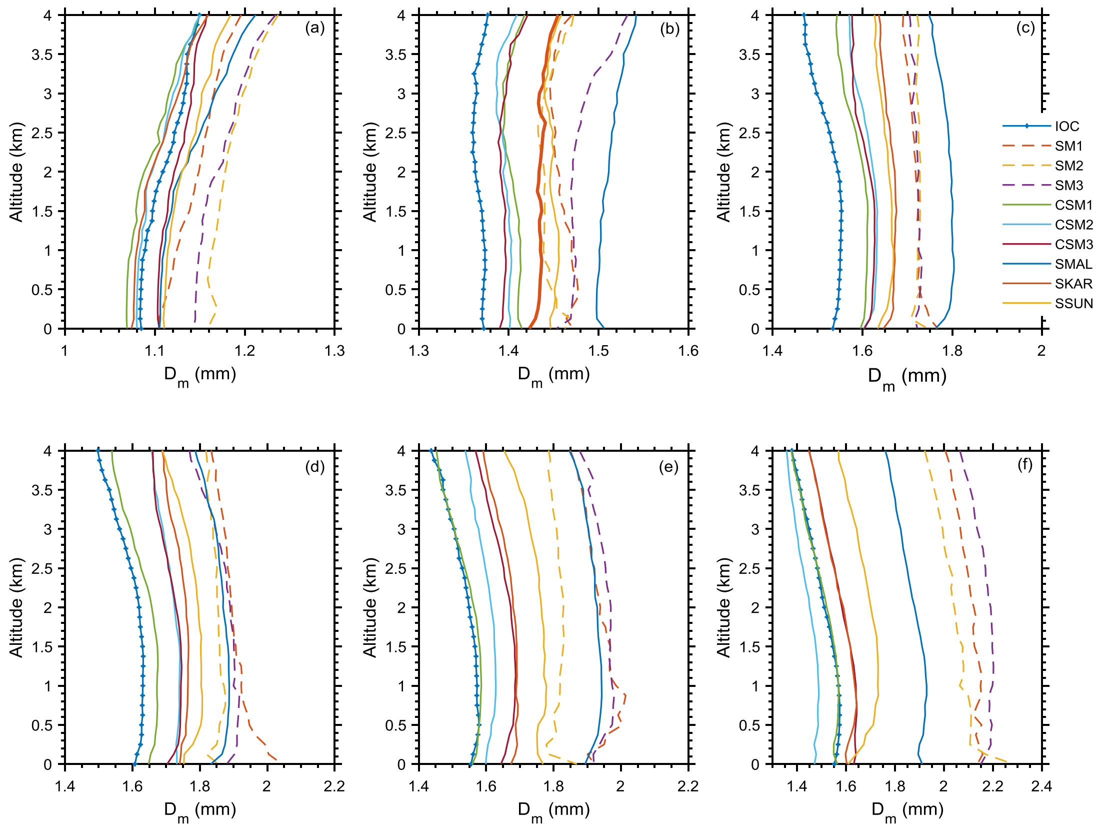

Figure 8. Vertical profile of mass-weight mean diameter (D_m) for ten selected locations of convective rain for a) very light rain, b) light rain, c) moderate rain, d) heavy rain, e) very heavy rain, and f) extreme rain.

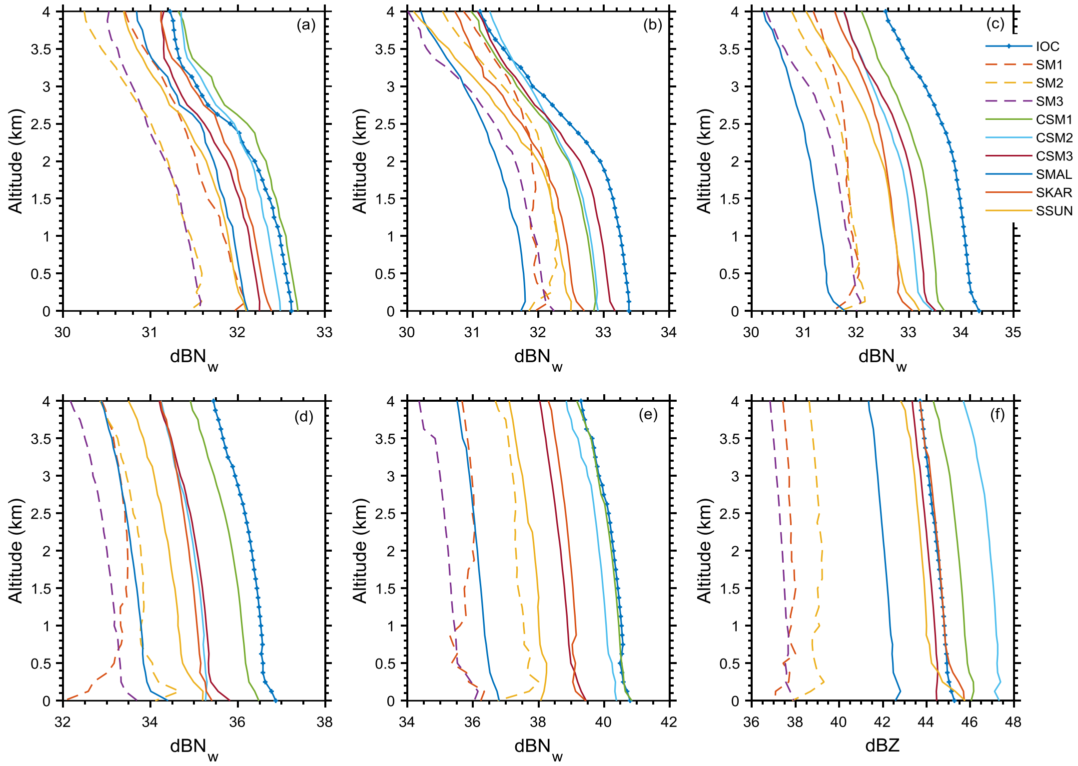

Figure 9. Vertical profile of total drop concentration (dBN_w,) for ten selected locations of convective rain for a) very light rain, b) light rain, c) moderate rain, d) heavy rain, e) very heavy rain, and f) extreme rain.

Figure 8 shows the vertical profile of D_m for convective rain. It can be seen that the positive gradient of D_m for higher rain intensity is larger than others, consistent with the vertical profile of Z_e (Figure 7). Furthermore, the larger positive gradient of N_w was observed for the lower intensity of convective rain for all locations (Figure 9). This pattern contrasts with the pattern of N_w for stratiform rain in which a larger positive gradient is observed for higher rain intensity. A smaller D_m gradient in lower intensity (very light to light rain) is associated with a larger N_w gradient, indicating a more dominant break up process during raindrop's fall. The coalescence process becomes dominant when the rainfall intensity increases, which can be seen from the increase of the D_m gradient and the decrease of N_w gradient.

The largest D_m was observed over land, and the lowest one was observed over offshore (IOC). Such contrast is more obvious for a higher rain intensity. A larger D_m over land is associated with its smaller gradient in the rain column (Figure 3). Thus, intense convective rain, which is indicated by larger Z_e (Figure 7), having larger drops (indicated by large D_m), is dominant over land. This is consistent with the variability of intense convective study in the tropical region [38, 46]. A larger D_m value was also observed over the Malacca strait (SMAL area). Intense convective rain is also frequently generated in this region [47]. The vertical profile of N_w for convective rain is similar to stratiform rain. The largest N_w value is observed over offshore (IOC), and the smallest one is observed over land (Figure 8). Thus, the DSD of convective rain over land comprises more large-sized drop concentration with a small number of raindrop total, as observed during stratiform rain.

4- Conclusion

This study reinforces the regional variation and rain type dependence of the vertical profile of precipitation over Sumatra. The DSD over land comprises more large-sized raindrop concentration with a small number of raindrop total, indicated by a larger D_m and smaller N_w over land than over the ocean. The land-ocean contrast of raindrop growth is visible. For convective rain, the increase of large-sized drops over the ocean is more significant than over land, indicated by a larger positive D_m gradient toward the surface. On the other hand, the reduction rate of large size drop is more significant over the ocean than over land, indicated by a larger negative D_m gradient toward the surface. Z_e, D_m, and N_w's vertical profile is also dependent on the rainfall intensity, especially for convective rain. A smaller D_m gradient in lower rain intensity (very light to light rain) is associated with a larger N_w gradient, indicating a more dominant break up process during the raindrop's fall. The coalescence process becomes dominant when the rainfall intensity increases, which can be seen from the increase of D_m gradient and the decrease of N_w gradient. In this study, we also found the shortcoming of rain classification of the CSF module. Some profiles classified as convective by the CSF module may be stratiform, indicated by strong BB pattern in the melting layer. The DSD over Sumatra is influenced by diurnal, intra-seasonal, and seasonal variability of the atmosphere. The characteristics of the vertical profile of DSD in terms of these variabilities are being conducted and will be reported in other papers.

5- Declarations

5-1- Author Contributions

Conceptualization, R.R. and M.; methodology, R.R. and M.; software, R.R. and M.; validation, M., H. and R.R.; formal analysis, R.R.; investigation, R.R.; resources, R.R.; data curation, M.; writing—original draft preparation, R.R.; writing—review and editing, M.; visualization, R.R.; supervision, M. and H.; project administration, M.; funding acquisition, M. All authors have read and agreed to the published version of the manuscript.

5-2- Data Availability Statement

Publicly available datasets were analyzed in this study. This data can be found here: www.gpm.nasa.gov/data.

5-3- Funding

The present study was supported by 2020 Magister Thesis Research Grants from the Ministry of Research, Technology, and Higher Education (Contract no: T/11/UN.16.17/PT.01.03/PTM-Kebencanaan/2020).

5-4- Acknowledgements

Thanks to NASA for providing open-source GPM Level-2 data.

5-5- Conflicts of Interest

The authors declare that there is no conflict of interests regarding the publication of this manuscript. In addition, the ethical issues, including plagiarism, informed consent, misconduct, data fabrication and/or falsification, double publication and/or submission, and redundancies have been completely observed by the authors.

6- References

[1] Jameson, A.R., and A.B. Kostinski. “What is a Raindrop Size Distribution.” Bulletin of American Meteorological Society 82, no. 6 (2001): 1169-1177. doi:10.1175/1520-0477(2001)082%3C1169:WIARSD%3E2.3.CO;2.

[2] Tokay, A., and D.A. Short. “Evidence from tropical raindrop spectra of the origin of rain from statiform versus convective clouds.” J. Appl. Meteor. 35, (1996): 355– 371. doi:10.1175/1520-0450(1996)035<0355:EFTRSO>2.0.CO;2.

[3] Duhanyan, N., and Yelva Roustan. “Below-Cloud Scavenging by Rain of Atmospheric Gases and Particulates.” Atmospheric Environment 45, no. 39 (2011): 7201–7217. doi:10.1016/j.atmosenv.2011.09.002.

[4] Ruan, Zheng, Hu Ming, Jianli Ma, Runsheng Ge, and Lingen Bian. “Analysis of the Microphysical Properties of a Stratiform Rain Event Using an L-Band Profiler Radar.” Journal of Meteorological Research 28, no. 2 (2014): 268–280. doi:10.1007/s13351-014-3091-x.

[5] Jiang, H., M. Sano, and M. Sekine. "Weibull raindrop-size distribution and its application to rain attenuation." IEE Proceedings-Microwaves, Antennas and Propagation 144, no. 3 (1997): 197-200. doi:10.1049/ip-map:19971193.

[6] Marzuki, M., T. Kozu, T. Shimomai, W. L. Randeu, H. Hashiguchi, and Y. Shibagaki. “Diurnal Variation of Rain Attenuation Obtained From Measurement of Raindrop Size Distribution in Equatorial Indonesia.” IEEE Transactions on Antennas and Propagation 57, no. 4 (2009): 1191–1196. doi:10.1109/tap.2009.2015812.

[7] Das, S., A. Maitra, and Ashish K. Shukla. “Rain Attenuation Modeling In the 10-100 GHz Frequency using Drop Size Distributions For Different Climatic Zones In Tropical India.” Progress in Electromagnetics Research B 25 (2010): 211–224. doi:10.2528/pierb10072707.

[8] Coppens, D., and Z. S. Haddad. “Effects of Raindrop Size Distribution Variations on Microwave Brightness Temperature Calculation.” Journal of Geophysical Research: Atmospheres 105, no. D19 (2000): 24483–24489. doi:10.1029/2000jd900226.

[9] Uijlenhoet, R. “Raindrop Size Distributions and Radar Reflectivity–rain Rate Relationships for Radar Hydrology.” Hydrology and Earth System Sciences 5, no. 4 (2001): 615–628. doi:10.5194/hess-5-615-2001.

[10] Yuter, Sandra E., and Robert A. Houze Jr. "Measurements of raindrop size distributions over the Pacific warm pool and implications for Z–R relations." Journal of Applied Meteorology 36, no. 7 (1997): 847-867. doi:10.1175/1520-0450(1997)036<0847:MORSDO>2.0.CO;2.

[11] Atlas, D., and C. W. Ulbrich. "An observationally based conceptual model of warm oceanic convective rain in the tropics." Journal of Applied Meteorology 39, no. 12 (2000): 2165-2181. doi:10.1175/1520-0450(2001)040<2165:AOBCMO>2.0.CO;2.

[12] Ulbrich, C. W., and D. Atlas. “Microphysics of Raindrop Size Spectra: Tropical Continental and Maritime Storms.” Journal of Applied Meteorology and Climatology 46, no. 11 (2007): 1777–1791. doi:10.1175/2007jamc1649.1.

[13] Cha, J.W., K.H. Chang, S. S. Yum, and Y.J. Choi. "Comparison of the Bright Band Characteristics Measured by Micro Rain Radar (MRR) at a Mountain and a Coastal Site in South Korea." Advances in Atmospheric Sciences 26, no. 2 (2009): 211–221. doi:10.1007/s00376-009-0211-0.

[14] Marzuki, M., H. Hashiguchi, M. K. Yamamoto, S. Mori, and M. D. Yamanaka. "Regional Variability of Raindrop Size Distribution over Indonesia." Annales Geophysicae 31, no. 11 (2013): 1941–1948. doi:10.5194/angeo-31-1941-2013.

[15] Hong, Song-You, and Ji-Woo Lee. "Assessment of the WRF Model in Reproducing a Flash-Flood Heavy Rainfall Event over Korea." Atmospheric Research 93, no. 4 (2009): 818–831. doi:10.1016/j.atmosres.2009.03.015.

[16] Ramadhan, R., Marzuki, and Harmadi. "Vertical structure of raindrop size distribution over West Sumatera from global precipitation measurement (GPM) observation". Journal of Physics: Conference Series. IOP Publishing, 2021. p. 012013. doi: doi:10.1088/1742-6596/1876/1/012013.

[17] Mori, S., Hamada J. I., Y. I. Tauhid, M. D. Yamanaka, N. Okamoto, F. Murata, N. Sakurai, H. Hashiguchi, and T. Sribimawati. "Diurnal land–sea rainfall peak migration over Sumatera Island, Indonesian Maritime Continent, observed by TRMM satellite and intensive rawinsonde soundings." Monthly Weather Review 132, no. 8 (2004): 2021-2039. doi:10.1175/1520-0493(2004)132<2021:DLRPMO>2.0.CO;2.

[18] Ramadhan, R., Marzuki, M. Vonnisa, Harmadi, H. Hashiguchi, and T. Shimomai. "Diurnal Variation in the Vertical Profile of the Raindrop Size Distribution for Stratiform Rain as Inferred from Micro Rain Radar Observations in Sumatra." Advances in Atmospheric Sciences 37, no. 8 (2020): 832–846. doi:10.1007/s00376-020-9176-9.

[19] Kozu, T., K. K. Reddy, S. Mori, M. Thurai, J. T. Ong, D. N. Rao, and T. Shimomai. "Seasonal and Diurnal Variations of Raindrop Size Distribution in Asian Monsoon Region." Journal of the Meteorological Society of Japan. Ser. II 84A (2006): 195–209. doi:10.2151/jmsj.84a.195.

[20] Ramadhan, R., Marzuki, Mutya V., Harmadi, H. Hashiguhci, and T. Shimomai. "Seasonal Variation in the Vertical Profile of the Raindrop Size Distribution for Stratiform Rain as Inferred from Micro Rain Radar Observations at Kototabang." The 1st International Conference on Physics and Applied Physics (THE 1ST ICP&AP) 2019: Fundamental and Innovative Research for Improving Competitive Dignified Nation and Industrial Revolution 4.0 (2020). doi:10.1063/5.0003181.

[21] Kozu, T., T. Shimomai, Z. Akramin, Marzuki, Y. Shibagaki, and H. Hashiguchi. "Intraseasonal Variation of Raindrop Size Distribution at Koto Tabang, West Sumatra, Indonesia." Geophysical Research Letters 32, no. 7 (2005): 1231-1249. doi:10.1029/2004gl022340.

[22] Hou, A. Y., R. K. Kakar, S. Neeck, A. A. Azarbarzin, C. D. Kummerow, M. Kojima, R. Oki, K. Nakamura, and T. Iguchi. "The Global Precipitation Measurement Mission." Bulletin of the American Meteorological Society 95, no. 5 (2014): 701–722. doi:10.1175/bams-d-13-00164.1.

[23] Marzuki, H. Hashiguchi, M. K. Yamamoto, M. Yamamoto, S. Mori, M. D. Yamanaka, R. E. Carbone, and J. D. Tuttle. "Cloud Episode Propagation over the Indonesian Maritime Continent from 10 years of Infrared Brightness Temperature Observations." Atmospheric Research 120–121 (2013): 268–286. doi:10.1016/j.atmosres.2012.09.004.

[24] Renggono, F., M. K. Yamamoto, H. Hashiguchi, S. Fukao, T. Shimomai, M. Kawashima, and M. Kudsy. "Raindrop Size Distribution Observed with the Equatorial Atmosphere Radar (EAR) During the Coupling Processes in the Equatorial Atmosphere (CPEA-I) Observation Campaign." Radio Science 41, no. 5 (2006). doi:10.1029/2005rs003333.

[25] Marzuki, H. Hashiguchi, T. Shimomai, I. Rahayu, M. Vonnisa, and Afdal. "Performance Evaluation of Micro Rain Radar over Sumatra through Comparison with Disdrometer and Wind Profiler." Progress In Electromagnetics Research M 50 (2016): 33–46. doi:10.2528/pierm16072808.

[26] Gorgucci, E., and L. Baldini. "Performance Evaluations of Rain Microphysical Retrieval Using Gpm Dual-Wavelength Radar by Way of Comparison With the Self-Consistent Numerical Method." IEEE Transactions on Geoscience and Remote Sensing 56, no. 10 (2018): 5705–5716. doi:10.1109/tgrs.2018.2824399.

[27] Chandrasekar, V., S. K. Biswas, M. Le, and H. Chen. "Cross Validation of Raindrop Size Distribution Retrievals from GPM Dual-Frequency Precipitation Radar Using Ground-Based Polarimetric Radar." IGARSS 2018- IEEE International Geoscience and Remote Sensing Symposium (2018): 8335-8338. doi:10.1109/igarss.2018.8518881.

[28] Petracca, M., L. P. D'Adderio, F. Porcù, G. Vulpiani, S. Sebastianelli, and S. Puca. "Validation of GPM Dual-Frequency Precipitation Radar (DPR) Rainfall Products over Italy." Journal of Hydrometeorology 19, no. 5 (2018): 907–925. doi:10.1175/jhm-d-17-0144.1.

[29] Kubota, T., N. Yoshida, S. Urita, T. Iguchi, S. Seto, R. Meneghini, J. Awaka, H. Hanado, S. Kida, and R. Oki. "Evaluation of Precipitation Estimates by at-Launch Codes of GPM/DPR Algorithms Using Synthetic Data from TRMM/PR Observations." IEEE Journal of Selected Topics in Applied Earth Observations and Remote Sensing 7, no. 9 (2014): 3931–3944. doi:10.1109/jstars.2014.2320960.

[30] Hamada, A., and Y. N. Takayabu. "Improvements in Detection of Light Precipitation with the Global Precipitation Measurement Dual-Frequency Precipitation Radar (GPM DPR)." Journal of Atmospheric and Oceanic Technology 33, no. 4 (2016): 653–667. doi:10.1175/jtech-d-15-0097.1.

[31] Awaka, J., M. Le, V. Chandrasekar, N. Yoshida, T. Higashiuwatoko, T. Kubota, and T. Iguchi. “Rain Type Classification Algorithm Module for GPM Dual-Frequency Precipitation Radar.” Journal of Atmospheric and Oceanic Technology 33, no. 9 (2016): 1887–1898. doi:10.1175/jtech-d-16-0016.1.

[32] Seto, S., and T. Iguchi. “Applicability of the Iterative Backward Retrieval Method for the GPM Dual-Frequency Precipitation Radar.” IEEE Transactions on Geoscience and Remote Sensing 49, no. 6 (2011): 1827–1838. doi:10.1109/tgrs.2010.2102766.

[33] Watters, D., A. Battaglia, K. Mroz, and F. Tridon. “Validation of the GPM Version-5 Surface Rainfall Products over Great Britain and Ireland.” Journal of Hydrometeorology 19, no. 10 (2018): 1617–1636. doi:10.1175/jhm-d-18-0051.1.

[34] Seto, S., T. Iguchi, and T. Oki. "The basic performance of a precipitation retrieval algorithm for the global precipitation measurement mission's single/dual-frequency radar measurements." IEEE Transactions on Geoscience and Remote Sensing 51, no. 12 (2013): 5239-5251. doi:10.1109/TGRS.2012.2231686.

[35] Tokay, A., L. P. D’Adderio, F. Porcù, D. B. Wolff, and W. A. Petersen. “A Field Study of Footprint-Scale Variability of Raindrop Size Distribution.” Journal of Hydrometeorology 18, no. 12 (2017): 3165–3179. doi:10.1175/jhm-d-17-0003.1.

[36] Le, M., and V. Chandrasekar. “An Algorithm for Drop-Size Distribution Retrieval from GPM Dual-Frequency Precipitation Radar.” IEEE Transactions on Geoscience and Remote Sensing 52, no. 11 (2014): 7170–7185. doi:10.1109/tgrs.2014.2308475.

[37] Huffman, G. J., D. T. Bolvin, D. Braithwaite, K. Hsu, R. Joyce, P. Xie, and S. H. Yoo. "NASA global precipitation measurement (GPM) integrated multi-satellite retrievals for GPM (IMERG)." Algorithm Theoretical Basis Document (ATBD) Version 4 (2015): 26.

[38] Yusnaini, H., and. Marzuki. “Vertical Distribution of Radar Reflectivity Factor in Intense Convective Clouds over Indonesia.” KnE Engineering 1, no. 2 (2019): 141-147. doi:10.18502/keg.v1i2.4439.

[39] Marzuki, H. Hashiguchi, M. Vonnisa, and Harmadi. “Seasonal and Diurnal Variations of Vertical Profile of Precipitation over Indonesian Maritime Continent.” Engineering and Mathematical Topics in Rainfall (April 18, 2018): 71. doi:10.5772/intechopen.74044.

[40] Rulfová, Zuzana, and Jan Kyselý. “Disaggregating Convective and Stratiform Precipitation from Station Weather Data.” Atmospheric Research 134 (2013): 100–115. doi:10.1016/j.atmosres.2013.07.015.

[41] Rosenfeld, D., and C. W. Ulbrich. “Cloud Microphysical Properties, Processes, and Rainfall Estimation Opportunities.” Radar and Atmospheric Science: A Collection of Essays in Honor of David Atlas. American Meteorolgy Society. (2003): 237–258. doi:10.1007/978-1-878220-36-3_10.

[42] Marzuki, H. Hashiguchi, T. Shimomai, I. Rahayu, M. Vonnisa, and Afdal. “Performance Evaluation of Micro Rain Radar over Sumatra through Comparison with Disdrometer and Wind Profiler.” Progress In Electromagnetics Research M 50 (2016): 33–46. doi:10.2528/pierm16072808.

[43] Wang, H., H. Lei, and J. Yang. “Microphysical Processes of a Stratiform Precipitation Event over Eastern China: Analysis Using Micro Rain Radar Data.” Advances in Atmospheric Sciences 34, no. 12 (2017): 1472–1482. doi:10.1007/s00376-017-7005-6.

[44] Bringi, V. N., V. Chandrasekar, J. Hubbert, E. Gorgucci, W. L. Randeu, and M. Schoenhuber. "Raindrop size distribution in different climatic regimes from disdrometer and dual-polarized radar analysis." Journal of the atmospheric sciences 60, no. 2 (2003): 354-365. doi:10.1175/1520-0469(2003)060<0354:RSDIDC>2.0.CO;2.

[45] Zhang, Aoqi, and Yunfei Fu. "The structural characteristics of precipitation cases detected by dual-frequency radar of GPM satellite." Chin. J. Atmos. Sci 42 (2018): 33-51.

[46] Kumar, S., and G. S. Bhat. “Vertical Profiles of Radar Reflectivity Factor in Intense Convective Clouds in the Tropics.” Journal of Applied Meteorology and Climatology 55, no. 5 (2016): 1277–1286. doi:10.1175/jamc-d-15-0110.1.

[47] Chen, H., P. M. Rizzoli, T.Y. Koh, and G. Song. “The Relative Importance of the Wind-Driven and Tidal Circulations in Malacca Strait.” Continental Shelf Research 88 (2014): 92–102. doi:10.1016/j.csr.2014.07.012.